Scientific Research Publishing

Journal of Modern Physics, 2025, 16(5), 754-773
https://www.scirp.org/journal/jmp
ISSN Online: 2153-120X
ISSN Print: 2153-1196

Equatorial Ionization Anomaly (EIA) under the Solar Radiation Spectrum

Abdoul Kader Segda[1,2*], Salfo Kaboré[1,2], Aristide Gybre[1,2], Frédéric Ouattara[1,2]

[1]Laboratory of Analytical Chemistry, Space Physics and Energy (LACAPSE), Koudougou, Burkina Faso
[2]Department of Physics, Norbert ZONGO University (UNZ), Koudougou, Burkina Faso
Email: *ksegda1@gmail.com

How to cite this paper: Segda, A.K., Kaboré, S., Gybre, A. and Ouattara, F. (2025) Equatorial Ionization Anomaly (EIA) under the Solar Radiation Spectrum. *Journal of Modern Physics*, **16**, 754-773.
https://doi.org/10.4236/jmp.2025.165041

Received: February 25, 2025
Accepted: May 27, 2025
Published: May 30, 2025

Abstract

This article aims to provide an answer to the equatorial or geomagnetic anomaly solely from the spectrum or power of solar radiation. Thus, each latitude at the level of the ionosphere would have a quasi-constant power around which the fluctuations in the power of solar radiation occur. Its quasi-constancy would be due to the fact that its amplitude fluctuations would be very negligible compared to those of the power of solar radiation so as not to break its sinusoidal shape and while allowing the resolution of the geomagnetic anomaly. This power of solar radiation dependent on latitude is a sinusoid with on the one hand maxima observed at 13˚ North latitude and 13˚ South latitude and on the other hand a minimum centered at the magnetic equator of latitude 0˚. Such a sinusoidal shape allows justifying the dome structure for the HmF2 altitudes and the gutter structure for the NmF2 ion density centered on the magnetic equator in magnetically calm periods of both foF2 and TEC. However, by taking into account these fluctuations and considering that the latitudinal powers observed in the Northern hemisphere are in "advance" of phase on those in the Southern hemisphere, the other characteristics of the equatorial anomaly in magnetically disturbed periods find answers. Such as the general symmetry of the crests when the latitudinal powers in the North are equal to those in the South, the asymmetry when in the North they are different from those in the South and finally the inverse fountain effect when the latitudinal powers at the equator or those close to the equator tend to prevail or prevail over the latitudinal powers in the North and South located at the latitudes of maximum density or very close to them. Finally, hourly and monthly ranges of symmetries and asymmetries, of tightening of the anomaly or of the equator effect have been identified, thus allowing better navigation and better performance of telecommunications tools.

Keywords

Anomaly, Ionization, Equatorial, Spectrum, Solar, NmF2, HmF2

1. Introduction

The sun, through its radiation and in its spectral part ranging from UVE to X-rays, contributes significantly to ionization in the ionosphere. The power of this radiation varies considerably in correlation with solar activity. For example, during an eruption, ionization in the ionosphere intensifies and absorption in the D region occurs. However, from this correlation observed with solar activity, the power of the transmitted solar radiation which will be at the origin of photoionization will also depend on the one hand on the position of the Earth in its daily rotation and on the other hand on its position in its movement of revolution throughout the months or year around the Sun. This variability in the transmitted power of solar radiation will also be, by extension, significantly responsible for the variability of the critical frequencies foF2, its peaks as much of maximum densities NmF2 as of its maximum observation heights HmF2 of these peaks of maximum densities NmF2 of the F2 sub-layer of the ionosphere. It is therefore in view of these predominant factors notwithstanding the processes of losses by recombination and transport and the influence of variations in the magnetic field, the electric field, the wind farm, etc. that we propose to carry out an analysis on the equatorial ionization anomaly under the prism of the solar radiation spectrum and to provide answers to further clarify this phenomenon. Indeed the low-latitude ionosphere, called the equatorial ionosphere, presents a particular configuration called the equatorial ionization anomaly (EIA) [1] or Appleton anomaly [2] and a theory called the equatorial fountain was developed for this purpose to provide clarification. From this theory, it emerges that the vector product of the ionospheric currents called equatorial electrojets (EEJ) [3] with the Earth's magnetic field will be at the origin of the rise in ionization also called vertical drift. This drift takes effect from the lower layers to high altitudes where they subsequently diffuse through magnetic field lines to descend into the depths of the F2 sublayer and reinforce the ionization of the equator magnetic field toward the tropics. Thus, to do this, the approach consists of presenting the data, the methodology used and, finally, the results discussion section to present the theory of the fountain effect and our results while discussing them to clarify the answers provided from the perspective of solar radiation.

2. Data

The data used are the critical frequencies foF2 from *in situ* measurements of the Djibouti (latitude 11.5˚N, longitude 42.8˚E), Ouagadougou (latitude 12.5˚N, lon-

gitude 358.5˚E) and Dakar (latitude 14.8˚N, longitude 342.6˚E) stations of the solar cycle 20 and ionograms from the Ionospheric Research Group (GRI/NTP/59) [4]. Also to compensate for the lack of detailed quantitative data or specific measurements and to further strengthen the credibility of this manuscript we used the IRI-2020 (International Reference Ionosphere) database which generates in addition to data, the graphical variability of many ionospheric parameters. And in this specific case of this manuscript of foF2, TEC, NmF2 and HmF2 both in temporal and latitudinal variability. The variability curves of the *in situ* measurements are averages resulting from the compilation of the *in situ* measurements of the entire cycle.

3. Methodology

The methodology consists of first presenting the equatorial fountain theory used to explain equatorial ionization anomaly patterns. These patterns will be illustrated by graphs of latitudinal variabilities of NmF2 and HmF2, both from diagrams of the Ionospheric Research Group (GRI/NTP/59) and from IRI-2020. Also, diurnal and monthly variabilities of foF2 will be illustrated, both from *in situ* measurements and from IRI-2020. Thus, after this presentation of the equatorial fountain theory, a proposal for analyzing the EIA using a mathematical model will be made. A mathematical model [5] [6] that has been effective, through its temporal solar radiation power component, in temporal analyses of seasonal or monthly variability of foF2 and its variabilities diurnal. This temporal component took into account the effects of rotation and revolution of the Earth by a power of solar radiation noted $P_0(t)$, ionization enhancement by SFEs, solar winds, CMEs by $P_{Solarflare}(t)$ and losses by recombination and transport mechanisms by $P_{Loss}(t)$. Thus, the time component will be given by the formula:

$$P_S(t) = P_0(t) + P_a(t) + P_{Solarflare}(t) - P_{Loss}(t) \tag{1}$$

$$P_0(t) = 2\sin\left(\frac{\pi}{12}t\right)\cos\left(\frac{\pi}{6}t\right) \tag{2}$$

If for example the time t in the formula of $P_0(t)$ is in time we will obtain the diurnal variation profiles of foF2 taking into accounts its very good correlation with solar radiation. For example, **Figure 1** obtained by varying $P_0(t)$ around an average of 10 also illustrates the variability profile of foF2.

The emphasis will however be placed on its latitudinal power component $P_s(\varphi)$ in order to formulate its mathematical expression which will be able to justify the configurations of the EIA. For this, postulates or hypotheses will be formulated there based on observation of the structure of NmF2 and HmF2 altitudes. Thus, 1) the more powerful the ionizing solar radiation, the more penetrating it is and the lower the HmF2 altitude to observe the NmF2 ionization maximum. 2) The less powerful the ionizing solar radiation, the higher the HmF2 observation altitude.

Thus, based on the observations of these different ionograms and many others, it

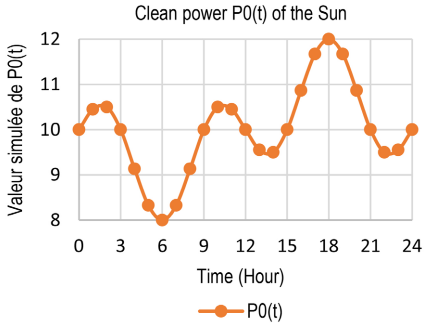

Figure 1. Example of diurnal profile of P0(t).

appears that the more powerful the ionizing solar radiation is, the more penetrating it is, and the lower the HmF2 altitude for observing the NmF2 ionization maximum is. The less powerful the ionizing solar radiation is, the higher the HmF2 observation altitude of the NmF2 ionization maximum. Such an observation seems to be more true if we observe Variations in (a) foF2 and (b) HmF2 values at the Jeju ionosonde (Northeast Asia) given by **Figure 2** during the G3-level geomagnetic storm occurring on November 3 and 4, 2021, which are extracted from the work of [7]. The blue dotted line (a) shows the highest electron density values of the IRI-2020 model with MSIS 2.1 on both calm and stormy days, while in (b) it represents the maximum height of the IRI-2020 model with MSIS 2.1 on each day.

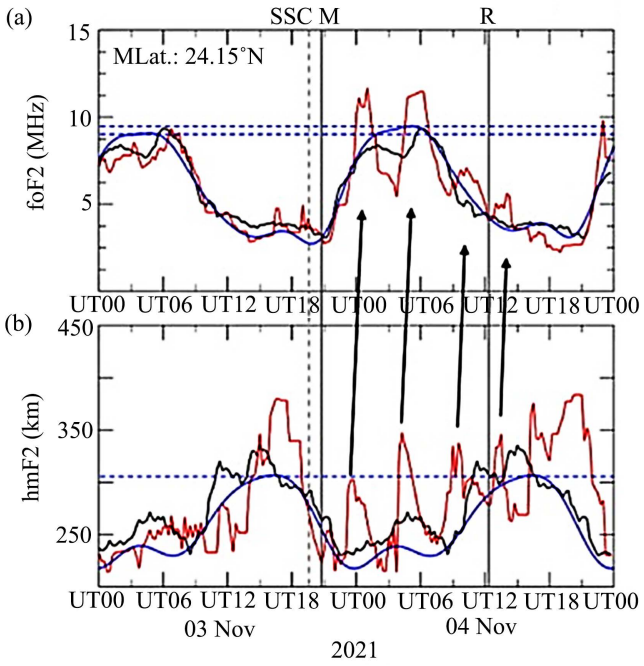

https://ars.els-cdn.com/content/image/1-s2.0-S0273117724007282-gr8.jpg

Figure 2. Variations of (a) foF2 and (b) HmF2 values at the Jeju ionosonde (Northeast Asia). Color BLACK ionosonde (quiet). Color RED ionosonde (storm). Color BLUE IRI-2020 MSIS 2.1.

3) Each latitude at the level of the ionosphere would present a quasi-constant latitudinal power of solar radiation which would fluctuate around the power of temporal solar radiation responsible for the biannual anomalies [8] [9].

The component $P_S(\varphi)$ of the latitudinal variation in ionizing solar radiation for a given latitude would be a quasi-constant and increase from the magnetic equator to the peaks of the maxima of ionization density, allowing us to justify the periods of magnetic calmness of the gutter structure of the maxima of isoionic densities and in a dome in the altitude HmF2 of these maxima of the isoionic densities NmF2, as shown by **Figure 3** stations of Djibouti (latitude 11.5˚N, longitude 42.8˚E), Ouagadougou (latitude 12.5˚N, longitude 358.5˚E) and Dakar (latitude 14.8˚N, longitude 342.6˚E) during the winter solstice period at the peak of the spring equinox (January, February, March) and the period from the peak of the autumnal equinox to the winter solstice (October, November and December) during the solar cycle 20.

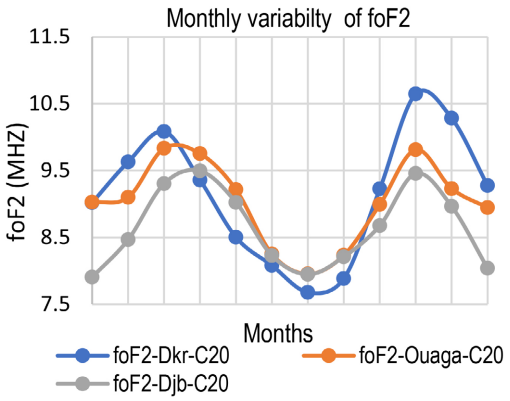

Figure 3. Monthly variation in foF2.

However, the power $P_S(\varphi)$ observed at each latitude would fluctuate with a negligible amplitude compared to that of $P_s(t)$ to preserve its sinusoidal shape while making it possible to justify the structure of the ionosphere during magnetically disturbed times, which tends, on the one hand, to a tightening of the anomaly toward the equator, as shown in **Figure 3**, during the periods from the peak of the spring equinox to the peak of the autumn equinox (March to October), which can progress as far as the formation of a single unique ridge above the magnetic equator, as shown in **Figure 3**, and, on the other hand, to the asymmetry of the ionization density of the two peaks. Overall, we deduce that ionizing solar radiation is increasingly powerful from the magnetic equator to the peak of maximum ionization density at geographic latitudes of 20˚N and 20˚S. Therefore, at a latitude φ, the power of ionizing solar radiation $P_S(\varphi,t)$ will present two components, one of which $P_S(t)$ will be that imparted to the temporal variation, which would vary around the component $P_S(\varphi)$ linked to latitude. We then note [5] [6]. That:

$$P_S(\varphi,t) = P_S(\varphi) + P_S(t) \tag{3}$$

Finally, as a limitation or weakness, the methodology is based on *in situ* measurements from a few stations and a few ionograms from the Research Group (GRI/NTP/59). However, this weakness was overcome by using data and graphics from the IRI-2020 model, which covers all latitudes.

4. Results and Discussion

4.1. Presentation of the Theory of the Equatorial Fountain

The equatorial ionosphere is the part of the ionosphere located above the magnetic equator over a strip of 600 km in the E sublayer located at 100 km altitude. This equatorial ionosphere has a particular configuration both in terms of the distribution of the ionic structure and the observation altitude of the isoionic maxima depending on the latitude, which is called the equatorial ionization anomaly (EIA).

1) Period of magnetic calm

Indeed, during times of magnetic calmness and at a certain time of day, two maximum ionization peaks called crests form on either side of the Northern and Southern Hemispheres geographically at latitudes of 20˚N and 20˚S. Followed by a progressive decrease in the ionization density to reach the ionization minimum peak at the 0˚ magnetic equator, thus forming a symmetry with respect to this magnetic equator called a structure in the gutter. We can observe the dome structure with HmF2 and the gutter structure with the foF2, Figure 4 and the TEC in Figure 5 in the latitudinal variation from the IRI-2020 model. The maximum ionization density peaks are obtained in this case at the geographic latitudes of −8˚ or 8˚S and 19˚ or 19˚N and the minimum at the geographic latitude of 9˚N.

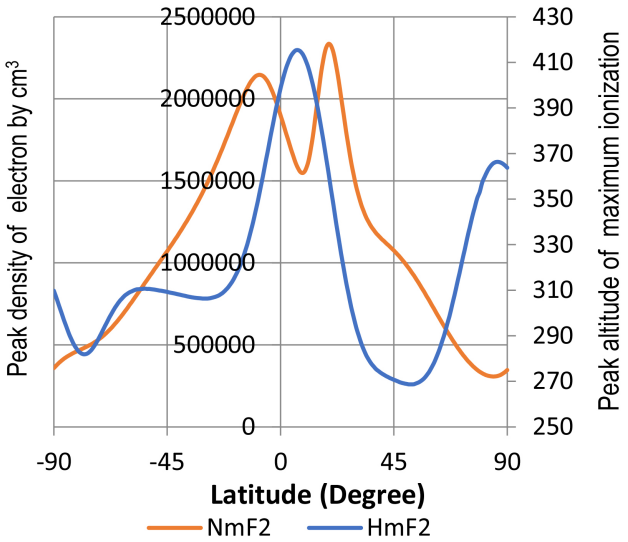

Figure 4. Dome structure (HmF2) and gutter (foF2)-IRI-2020.

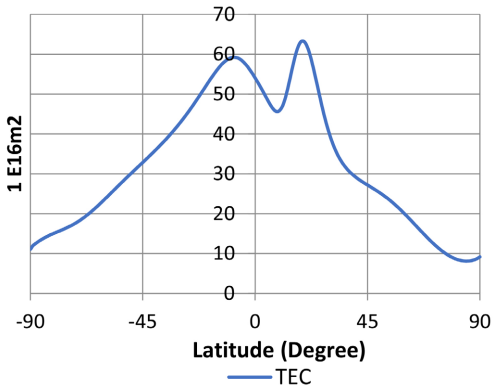

Figure 5. Gutter structure (TEC)-IRI-2020.

Also **Figure 6** shows an ionogram extracted from the work of the Ionospheric Research Group (GRI/NTP/59) by Lapouille, 1970, of the variation in density as a function of latitude for different fixed altitudes, with the maximum density NmF2 at each latitude indicating that this gutter structure occurs well. Parallel to this observation, the observation altitude of the isoionics is increasingly higher from the ionization ridge peaks to the ionization minimum peak at the magnetic equator, thus forming a dome structure, as shown in **Figure 7** [4].

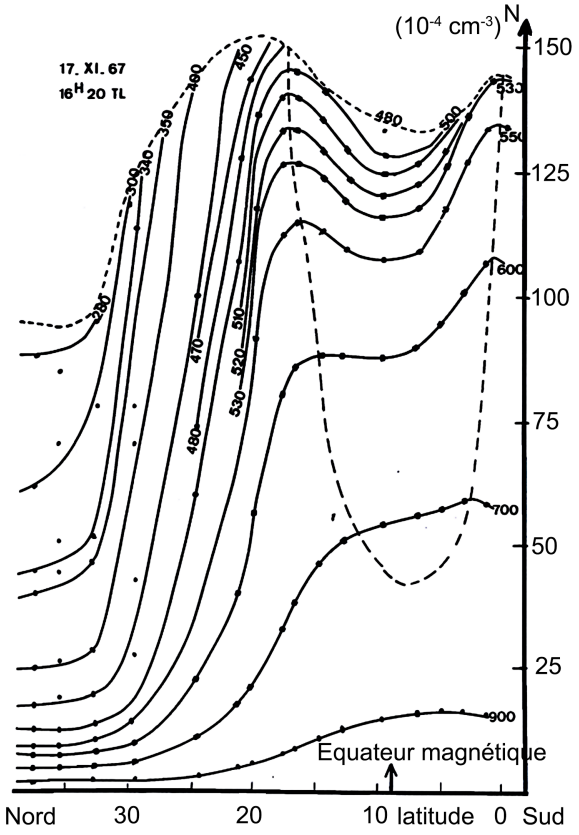

Figure 6. Density at constant altitude [4].

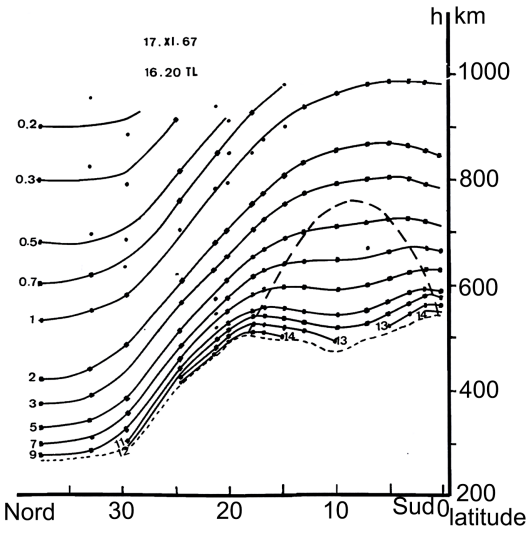

Figure 7. Altitude of isoionics [4].

2) Magnetic disturbance period

However, in times of major magnetic disturbance, we observe, on the one hand, a tightening of the anomaly toward the equator, which can occur as long as the formation of a unique maximum ionic density above the magnetic equator (**Figure 8** and **Figure 9**); on the other hand, there is the asymmetry in the ionization density of the two peaks.

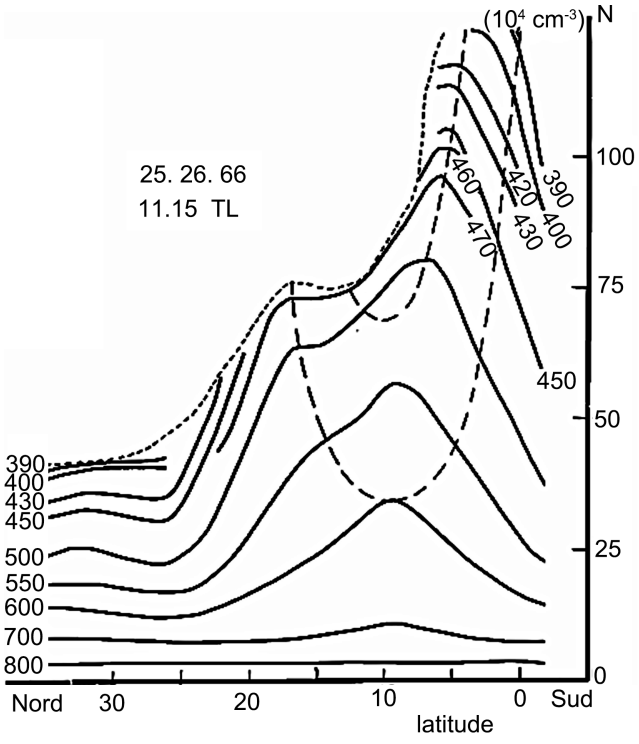

Figure 8. Density at constant altitude during magnetically disturbed times [4].

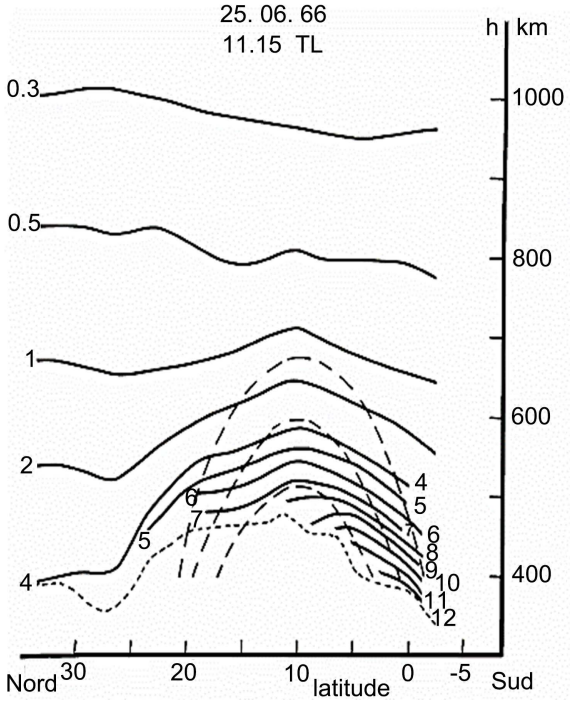

Figure 9. Altitude of isoionics at different magnetic disturbance times [4].

3) Equatorial fountain theory

As the iso-ionic maxima are aligned along the same magnetic field line, thus forming an arch, a theory called the "equatorial fountain effect" was developed to elucidate such an anomaly phenomenon. This theory is based on the equatorial electrojet (EEJ), which is an ionospheric electric current circulating from west to east with a field vector ($\boldsymbol{E}$). The vector product of such a field vector ($\boldsymbol{E}$) with the magnetic field vector ($\boldsymbol{B}$), which is horizontal to the equator and oriented toward the North, causes an increase in ionization at speed ($\boldsymbol{V}$) through the F2 sublayer, reinforcing the ionization in this part. To this end, we note the following:

$$\boldsymbol{V} = \frac{\boldsymbol{E} \wedge \boldsymbol{B}}{B^2} \tag{4}$$

Thus, at higher altitudes, particularly in region F, the ascent speed raises the ionospheric plasma to altitudes greater than 700 km, where the plasma meets magnetic field lines that connect the two hemispheres. From there, the plasma diffuses along the lines of magnetic force under the action of gravity and pressure gradients [10] [11]. And descends to the lowest altitudes to thus reinforce ionization in the tropics, thus justifying the gutter structure for isoionic densities and the dome structure for HmF2 altitudes for observing these isoionic maxima. This is the theory of the "equatorial fountain effect", as shown in **Figure 10**, used to justify the equatorial ionization anomaly (EIA). Since then, many studies have been carried out to validate this theory, particularly in determining the speed of increase in the plasma concentration.

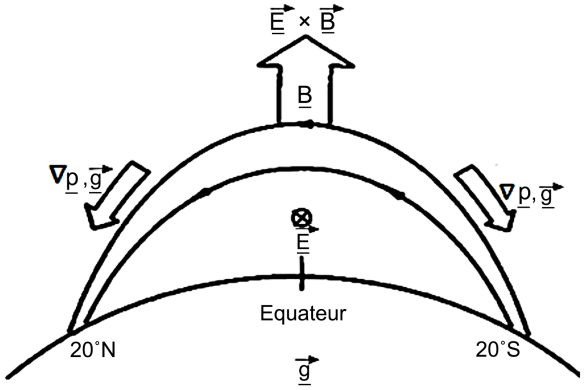

Figure 10. Schematic diagram of fountain formation [1].

4.2. Mathematical Model

The first problem to be solved was to propose a mathematical function capable of simulating the natural power observed at each latitude. The formulas found are on the one hand of the form

$$P_c(\varphi) = P_{c0} + \left(1 - \sin\left(\frac{3\pi}{40}(\varphi - 20)\right)\right) \tag{5}$$

and on the other hand

$$P_c(\varphi) = P_{c0} + \left(1 - \sin\left(\frac{3\pi}{40}(\varphi - (20 + \theta))\right)\right) \tag{6}$$

with θ the latitude corresponding to the magnetic equator. The first could be called the one leading to the geographic or magnetic anomaly (**Figure 11**) if we consider that the observed latitudes are expressed relative to the geographic or magnetic equator. The maxima in such a case are found at 13˚S and 13˚N.

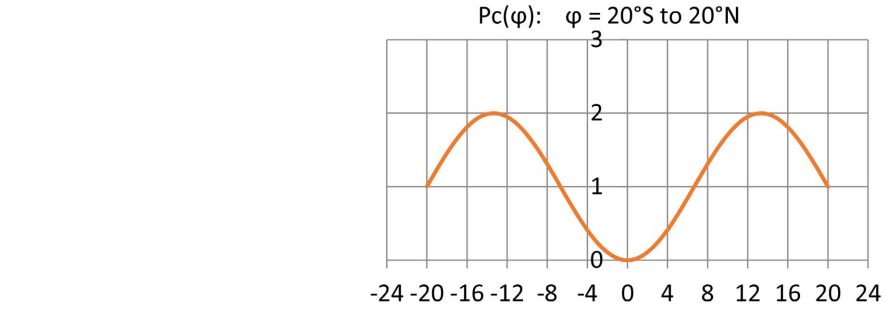

Figure 11. Variation of simulated latitudinal power. Maximum peak LAT 13˚S and 13˚N. Minimum peak LAT 0˚.

The second **Figure 12** is the one responding only to the geomagnetic anomaly because the minimum is centered at the geomagnetic equator at latitude θ° which does not correspond exactly to the geographic equator. The maximums in this case are observed at the geographic latitudes of 10˚S and 16˚N for example $\theta = 3^{\circ}$ but

still retaining the symmetry of 13˚S to 13˚N with respect to the magnetic equator.

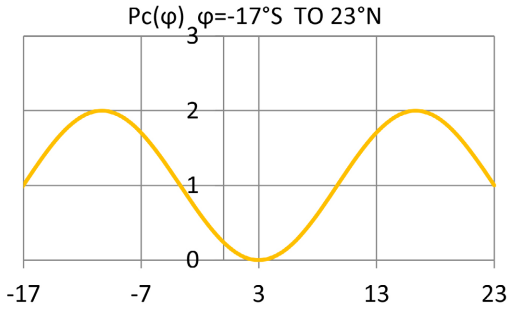

Figure 12. Variation of simulated latitudinal power. Maximum peak LAT 10˚S and 16˚N. Minimum peak LAT 3˚.

In any case, both formulas are effective for simulation because the objective sought for us would be to prove that without calling on the one hand on the cross effects of the currents [12] or ionospheric winds and the Earth's magnetic field and on the other hand magnetic field lines, the basis of the theory of the fountain effect we could explain this anomaly only by the power of solar radiation. This solar power which moreover allowed us to justify the semi-annual anomaly [10] [11] observed at each latitude. So for simplicity and especially since the real value of the magnetic equator would fluctuate depending on the periods we have opted for the first formula (**Figure 11**) considering that the latitudes are expressed in relation to the magnetic equator. Moreover, the $1-\sin\left(\frac{3\pi}{40}(\varphi-20)\right)$ in the expression of $P_c(\varphi)$ would be due to the fact that the value of the self-power for each latitude is positive so that to add to the component of the power of the solar radiation varying with time $P_S(t)$ and responsible for the semi-annual anomaly at a latitude φ This data will allow for an increasingly powerful solar radiation power, therefore increasingly penetrating from the equator to these latitudes corresponding to the ionization maxima. And for example, **Figure 13** at 10H and for each season.

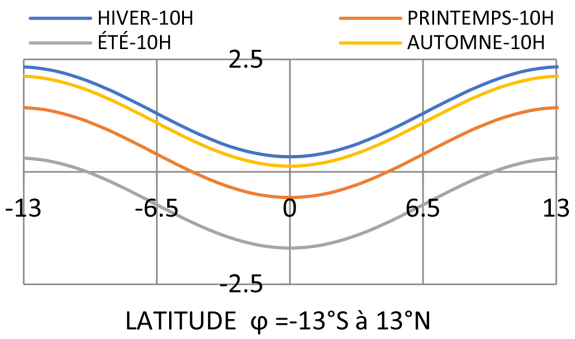

Figure 13. Simulated latitudinal power variation. Gutter structure by season Maximum peak LAT 13˚S to 13˚N. Minimum peak LAT 0˚.

Thus, for a season, at a given time and constant altitude (Figure 13) the ionization will be all the more pronounced as one moves away from the magnetic equator for latitudes of 13˚S and 13˚N. In parallel with this observation for the same ionization density or iso-ionic the observation altitude (Figure 14) will be even more pronounced when leaving the latitudes of the ionization maximum of 13˚S or 13˚N for the magnetic equator.

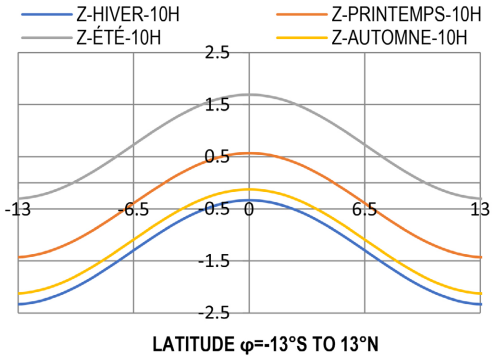

Figure 14. Simulated latitudinal power variation. Gutter structure by season Maximum peak LAT 13˚S to 13˚N. Minimum peak LAT 0˚.

We could therefore observe the dome structure for what concerns the altitudes and the gutter structure for what concerns the ionization density centered at the magnetic equator characteristic of the equatorial or geomagnetic anomaly in magnetically calm periods. This is concretely translated during the day by the diurnal profiles of the critical frequencies foF2 as shown by the curves in Figure 15 from the IRI-2020 model where the latitudes of −8˚ and 19˚ correspond to the latitudes of maximum density and the latitude of 9˚ corresponds to the magnetic equator. Indeed:

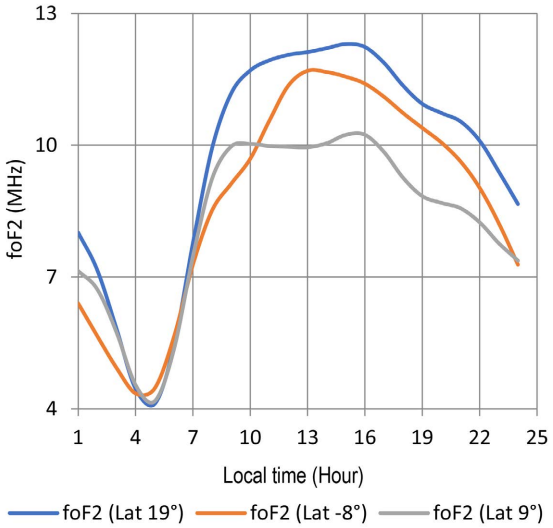

Figure 15. Diurnal profile foF2 of maximum density of latitude 19˚ IRI-2020.

1) On the one hand for the same latitude both in the Northern and Southern hemispheres the amplitudes of the critical frequencies foF2 are almost identical, that is to say of almost the same amplitudes, thus reflecting the symmetry of the peaks of maximum density.

2) On the other hand, the foF2 amplitudes are increasingly higher from the magnetic equator to the latitudes of maximum density. For example, the diurnal foF2 profiles at the latitudes of maximum density will be raised, therefore above those at the magnetic equator. For example, the maximum foF2 peaks are less than 12 MHz at the magnetic equator (Latitude 9˚) and greater than 12 MHz at the latitudes of maximum density (Latitude 19˚ and −8˚).

These different observations made with the foF2 frequencies are also made with the TEC at these different latitudes.

If beyond 700 km centered on the magnetic equator, the peak-trough structure tends to break up to become uniform, this could be explained on the one hand by the rarity of ionizable matter and on the other hand by the increasingly drastic decrease in electron density. This seems truer especially since the limit of the upper ionosphere beyond 1000 km is poorly known because it can "be seen as the place where it ends in the plasmasphere which is defined as the place where the density of neutrals is very low" [7].

Clean power $P_c(\varphi)$ observed at each latitude reflecting a physical reality would also be fluctuating. However, its fluctuation with regard to that of the power $P_s(t)$ responsible for the semi-annual anomaly is almost negligible, leading us to consider it as a quasi-constant. This also allowed us to justify certain main characteristics of the geomagnetic anomaly. However, by taking into account its fluctuations, although negligible, we could provide answers justifying, on the one hand, the breaking of symmetry or the asymmetry [13] [14] in the density and altitude of the two peaks and on the other hand the behavior in magnetically agitated weather which tends to tighten the anomaly towards the magnetic equator. In fact, the fluctuations in power $P_c(\varphi_N)$ and $P_c(\varphi_S)$ (**Figure 16**) respectively observed in the Northern and Southern hemisphere are in phase quadrature with $P_c(\varphi_N)$ in advance of $\frac{\pi}{2}$ on that of $P_c(\varphi_S)$. Of

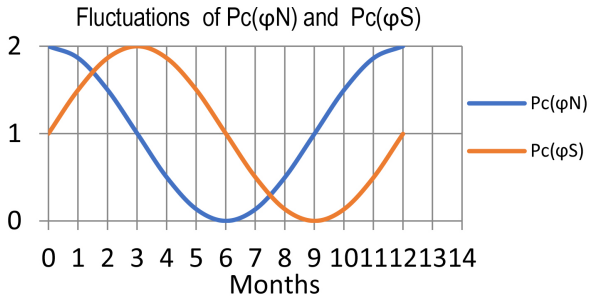

Figure 16. Simulated fluctuation of latitudinal powers in the Northern and Southern hemispheres IRI-2020.

course, one could also start from the fact that the $P_c(\varphi_S)$. Powers were ahead of those of the $P_c(\varphi_N)$ powers. This is therefore just to justify the asymmetries, the dissymmetries and the tightening of the anomaly.

Are therefore monthly fluctuations of the amplitude P_{c0} of $P_c(\varphi)$ north of the shape $P_{c0}(t)=k_0\left(1+\cos\left(\frac{\pi}{6}t\right)\right)$ (7) and south of the shape $P_{c0}(t)=k_0\left(1+\cos\left(\frac{\pi}{6}t-\frac{\pi}{2}\right)\right)$ (8). So if the fluctuation of one is at its maximum value the other is at its minimum value.

From these observations, we will have the strong propensity to observe the general or most perfect symmetry as much in density of ionization of the crests as in their altitudes as in mid-February and mid-August where the power $P_c(\varphi_N)=P_c(\varphi_S)$ (9) (**Figure 16** and **Figure 17**).

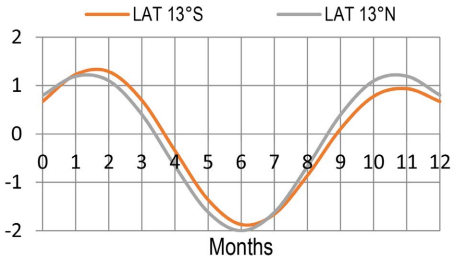

Figure 17. Simulated observation of symmetries and asymmetries in the monthly variability of foF2 LAT 13˚S and LAT 13˚N.

Outside of these periods $P_c(\varphi_N)\neq P_c(\varphi_S)$ (10) (**Figure 16** and **Figure 17**) and we will observe an asymmetry as much in terms of the ionization density as in the altitudes of the crests and this sometimes, in favor of the Northern hemisphere or that of the Southern hemisphere.

In fact, from the winter solstice in mid-February and from mid-August to the winter solstice we have $P_c(\varphi_N)>P_c(\varphi_S)$ (11) (**Figure 17**). As a result, we will always observe on the one hand an asymmetry in high ionization density of the two peaks in favor of the Northern hemisphere and on the other hand an asymmetry in altitude of these same peaks in favor of the Southern hemisphere where they will be the highest. This is also reflected on a daily basis in the diurnal variability of the critical frequencies foF2 as shown in **Figure 18** where we observe moments of quasi-symmetries and asymmetries of the two latitudes of maximum density 13˚N and 13˚S.

Thus, the moments of quasi-symmetries will be observed from 1 am to 2 am, from 7 am to 8 am, from 1 pm to 2 pm, and from 7 pm to 8 pm. An asymmetry in the ionization density in favor of the Northern Hemisphere from 0 am to 1 am, from 8 am to 1 pm, and finally from 8 pm to 12 am. The other hourly intervals, the asymmetries in the ionization density are in favor of the Southern Hemisphere. That is, from 3 am to 7 am and from 2 pm to 7 pm.

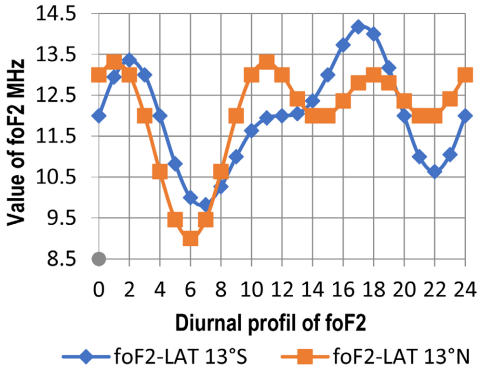

Figure 18. Diurnal profile foF2 during magnetic disturbance of maximum density of latitudes LAT 13˚N and LAT 13˚S.

Finally, if the fluctuations of the powers $P_c(\varphi)$ in magnetically disturbed periods are such that we observe an inverse process of the so-called magnetically calm periods, especially from June to the end of September where $P_c(\varphi_N)$ and $P_c(\varphi_S)$ (**Figure 19**) are jointly both at their lowest minimum at the point that $P_c(\varphi_E)$ or those of latitudes very close to the equator prevail over those of the density maxima we could justify the so-called inverse fountain effect which in our part is the magnetic equator effect $P_c(\varphi_E)$ (**Figure 19** and **Figure 20**).

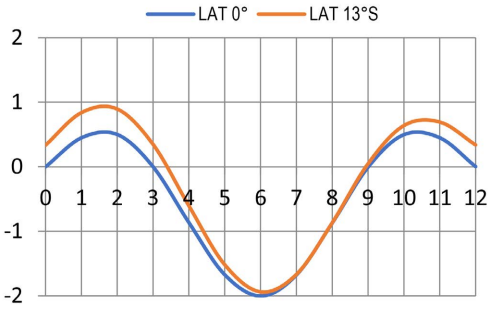

Figure 19. Tightening of the anomaly Diurnal profile foF2 during magnetic disturbance. Tightening of anomaly of maximum density of latitudes LAT 13˚N and LAT 13˚S with LAT 0˚.

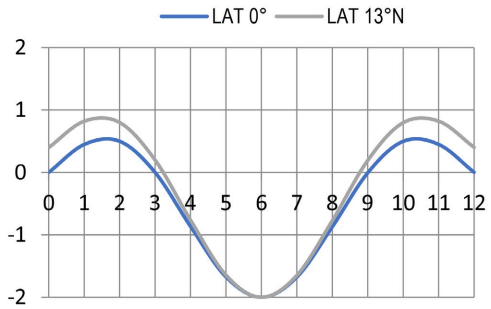

Figure 20. Tightening of the anomaly Diurnal profile foF2 during magnetic disturbance. Tightening of anomaly of maximum density of latitudes LAT 13˚N and LAT 13˚N with LAT 0˚.

In fact, the power of solar radiation will be less and less pronounced from the magnetic equator to latitudes 13˚S and 13˚N and consequently the ionization density at constant altitude will be all the more pronounced from these latitudes to the magnetic equator. Thus, for the same density or iso-ionic the altitudes will be all the higher from the magnetic equator to these latitudes. In a word, we will now observe the dome structure in relation to the ionization densities and the gutter structure in relation to the altitudes of the iso-ionics centered at the magnetic equator. This is concretely reflected in the diurnal variability by a tightening at a certain moment of the foF2 of the magnetic equator to those of the latitudes of maximum density as shown in Figure 21.

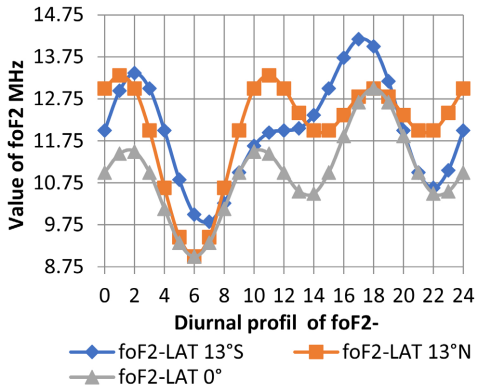

Figure 21. Diurnal profile foF2 during magnetic disturbance. Resserrement of anomaly of maximum density of latitudes LAT 13˚N and LAT 13˚S with LAT 0˚.

Thus we can observe the tightening of the LAT 0˚ and LAT 13˚N anomaly around 4 am to 8 am and around 17 pm to 20 pm. A tightening of the LAT 0˚ and LAT 13˚S anomaly around 8 am to 10 am and from 20 pm to 22 pm. Also if the magnetic disturbance is very important we can observe that at times the ionization densities at the equator or towards the equator prevail over those of the crests of the latitudes of maximum ionization density, for example Figure 22.

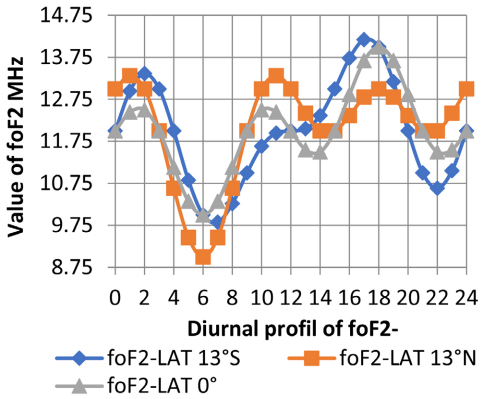

Figure 22. Diurnal profile foF2 during magnetic disturbance. Equator effect of anomaly of maximum density of latitudes LAT 13˚N and LAT 13˚S with LAT 0˚.

Thus, we can observe the equator effect where low latitudes prevail in ionization density. Ionization densities at LAT 0˚ prevail over LAT 13˚N around 3 am To 9 am and around 3 pm to 9 pm. Ionization densities at LAT 0˚ prevail over LAT 13˚S around 6 am to 12 pm and from 6 pm to 12 am. Finally, ionization densities at LAT 0˚ prevail over LAT 13˚N and 13˚S around 6 am to 9 am and 6 pm to 9 pm. Finally, if the equator effect allowed us to explain the tightening of the anomaly at the equator instead of the inverse fountain [15] [16], how would it be for the night peaks of the critical frequencies foF2 where the inverse fountain is also used to justify them?

To this end, we can always add that the night peaks of the critical frequencies foF2 would not be due to this effect. These night peaks would rather be induced by ionization corpuscular or particulate ionization that supplements the ionization induced by solar radiation observed during the day during the night. The mechanism of this ionization is such that it tends, through these effects, to strongly preserve the specific profile of the observed solar radiation. This ionization will be increasing if the profile is of the reverse R type and decreasing if it is of the morning peak M type. However, the corpuscular ionization, which should be increasing or decreasing depending on the period, will nevertheless experience a peak of the maximum ionization centered around 11 pm and midnight, due to the preponderance of losses caused by recombination and leakage or transport of electrons. Such a maximum can also, depending on the period, be observed a little earlier before 11 pm or a little later between midnight and 6 am. Thus the night peaks of the critical frequencies foF2 would therefore correspond to these instants or periods where the corpuscular ionization peak prevails over the losses and not to a reinforcement induced by the inverse fountain effect.

4.3. Importance of the Study

This study allowed us to analyze the equatorial ionization anomaly EIA through the solar radiation spectrum. A mathematical model as a basis for analysis with formulas was established for this purpose and taking into account: 1) The geographical position allowing the analysis of the EIA. 2) The rotation of the Earth allows the analyses of diurnal variability of critical frequencies foF2, TEC. 3) The revolution of the Earth around the Sun allows the analysis of monthly or seasonal variabilities. 4) The sunspot cycle allowing to justify the propensities for the formation of diurnal profiles B, M, R, D and P of foF2. 5) Solar flares, solar winds, CMEs losses by recombination and transport mechanism to explain the mechanisms of transformation of profiles into another profile. Also for the specific case of the EIA study, hourly and monthly ranges of symmetries and asymmetries between the Northern and Southern hemispheres were identified as well as the periods of tightening of the anomaly or the equator effect. Thus, in-depth knowledge of these meteorological events would allow better navigation and further improve telecommunication tools such as GPS through better calibrations. In summary,

the proposed mathematical model is a powerful tool for analyzing ionospheric phenomena and can be important in many other fields.

4.4. Outlook

At the end of this study, we plan to carry out an analysis of the nocturnal variability of critical frequencies foF2 and TEC.

5. Conclusion

At the end of this article, we can say that the objective sought to solve the problem of the equatorial or geomagnetic ionospheric anomaly only by the power or by the spectrum of the solar radiation is achieved. The structure of day in magnetically calm weather, the asymmetry in the density and the altitude and the behavior in magnetically agitated weather have found answers. These answers are observed as well in the monthly or seasonal variations as in the diurnal variations. This power of the solar radiation in question has two components. The one fluctuating in time which makes it possible to explain the semi-annual anomaly, the equinoctial asymmetries, the different diurnal profiles and the fluctuating one in space which represents the proper power for a given latitude or also the variation of the power of the solar radiation from the magnetic equator to this latitude.

Acknowledgements

The authors would like to thank all the material or immaterial contributions, provision of resources or others that contributed, on the one hand, to the writing of the article and, on the other hand, to the submission and acceptance of the article.

Conflicts of Interest

The authors declare no conflicts of interest regarding the publication of this paper.

References

[1] Kelley, M.C. (1989) The Earth's Ionosphere, Plasma Physics and Electrodynamics. 2nd Edition, Academic Press.

[2] Appleton, E.V. (1946) Two Anomalies in the Ionosphere. *Nature*, **157**, 691-691. https://doi.org/10.1038/157691a0

[3] Untiedt, J. (1967) A Model of the Equatorial Electrojet Involving Meridional Currents. *Journal of Geophysical Research*, **72**, 5799-5810. https://doi.org/10.1029/jz072i023p05799

[4] Lapouille, A. (1970) Groupe de Recherches Ionosphériques (GRI)/NTP/59-Quelques résultats expérimentaux de l'Ionosphère Equatoriale Africaine, 1970.

[5] Abdoul-Kader, S., Doua Allain, G. and Salfo, K. (2023) Contribution to the Explanation of the Semi-Annual Anomaly Observed in the Intertropical Zone Using the Critical Frequencies foF2 Extracted during the Sunspot Cycles 20, 21 and 22 at the Ouagadougou Station. *International Journal of Advanced Research*, **11**, 412-417. https://doi.org/10.21474/ijar01/16266

[6] Abdoul-Kader, S., Allain, G.D. and Aristide, G. (2023) New Analysis of the Seasonal Variation of the Critical Frequencies foF2 by a Proposed Formula of the Power of Solar Radiation. *International Journal of Geophysics*, **2023**, Article ID: 4405266. https://doi.org/10.1155/2023/4405266

[7] Kim, J. and Kwak, Y. (2025) Validating the IRI-2020 Model for Ionospheric Storms over the Northeast Asian Sector Induced by Extreme Geomagnetic Storms. *Advances in Space Research*, **75**, 4347-4369. https://doi.org/10.1016/j.asr.2024.07.032

[8] Huang, Y. and Cheng, K. (1996) Solar Cycle Variations of the Equatorial Ionospheric Anomaly in Total Electron Content in the Asian Region. *Journal of Geophysical Research*: *Space Physics*, **101**, 24513-24520. https://doi.org/10.1029/96ja01297

[9] Araujo-Pradere, E.A. (1997) Fof2 Frequency Bands in El Cerrillo, Mexico during Magnetically Quiet Conditions. *Revista Brasileira de Geofísica*, **15**, 161-164. https://doi.org/10.1590/s0102-261x1997000200006

[10] Martyn, D.F. (1947) Atmospheric Tides in the Ionosphere, I. Solar Tides in the F2 Region. *Proceedings of the Royal Society of London A*, **89**, 241-260.

[11] Duncan, R.A. (1960) The Equatorial F-Region of the Ionosphere. *Journal of Atmospheric and Terrestrial Physics*, **18**, 89-100. https://doi.org/10.1016/0021-9169(60)90081-7

[12] Spreiter, J.R. and Briggs, B.R. (1961) Theory of Electrostatic Fields in the Ionosphere at Equatorial Latitudes. *Journal of Geophysical Research*, **66**, 2345-2354. https://doi.org/10.1029/jz066i008p02345

[13] Bramley, E.N. and Peart, M. (1965) Diffusion and Electromagnetic Drift in the Equatorial F2-Region. *Journal of Atmospheric and Terrestrial Physics*, **27**, 1201-1211. https://doi.org/10.1016/0021-9169(65)90081-4

[14] Bramley, E.N. and Young, M. (1968) Winds and Electromagnetic Drifts in the Equatorial F2-Region. *Journal of Atmospheric and Terrestrial Physics*, **30**, 99-111. https://doi.org/10.1016/0021-9169(68)90044-5

[15] Rishbeth, H. (1971) The F-Layer Dynamo. *Planetary and Space Science*, **19**, 263-267. https://doi.org/10.1016/0032-0633(71)90205-4

[16] Fejer, B.G., Farley, D.T., Woodman, R.F. and Calderon, C. (1979) Dependence of Equatorial *f* Region Vertical Drifts on Season and Solar Cycle. *Journal of Geophysical Research*: *Space Physics*, **84**, 5792-5796. https://doi.org/10.1029/ja084ia10p05792

Appendix: Summary of the Formulas of the Mathematical Model

1) The equation gives an explanation for the different anomalies, asymmetries and diurnal profiles (B, M, R, D and P) of the foF2.

2) The equation gives an explanation of the equatorial ionization anomaly in times of magnetic calm.

3) The equation gives an explanation of the equatorial ionization anomaly in times of magnetic calm.

4) The equation gives an explanation of the equatorial ionization anomaly in times of magnetic disturbance at latitudes of the Northern Hemisphere.

5) The equation gives an explanation of the equatorial ionization anomaly in times of magnetic disturbance at latitudes in the Southern Hemisphere.

$$\begin{cases} (1) \to P_S(t) = 2P_{\alpha 0} \sin\left(\frac{\pi}{12}t\right)\cos\left(\frac{\pi}{6}t\right) + P_a(t) + P_{Solarflare}(t) - P_{Loss}(t) \to P_{\alpha 0} = 1 \text{ or } P_{\alpha 0} \neq 1 \\ (2) \to P_S(\varphi, t) = P_{c0} + \left(1 - \sin\left(\frac{3\pi}{40}(\varphi - 20)\right)\right) + P_S(t) \to P_{c0} + 1 \text{ is adjusted to the measured average value} \\ (3) \to P_S(\theta, \varphi, t) = P_{c0} + \left(1 - \sin\left(\frac{3\pi}{40}(\varphi - (20 + \theta))\right)\right) + P_S(t) \\ (4) \to P_S(\varphi, t)_N = k_0\left(1 + \cos\left(\frac{\pi}{6}t\right)\right) + \left(1 - \sin\left(\frac{3\pi}{40}(\varphi - 20)\right)\right) + P_S(t) \to k_0 = 1 \text{ or } k_0 \neq 1 \\ (5) \to P_S(\varphi, t)_S = k_0\left(1 + \cos\left(\frac{\pi}{6}t - \frac{\pi}{2}\right)\right) + \left(1 - \sin\left(\frac{3\pi}{40}(\varphi - 20)\right)\right) + P_S(t) \to k_0 = 1 \text{ or } k_0 \neq 1 \end{cases}$$